# LANGMUIR

pubs.acs.org/Langmuir Article

# Effects of Ion Concentration and Headgroup Chemistry on Thin Lipid Film Drainage

Oscar Zabala-Ferrera and Peter J. Beltramo\*



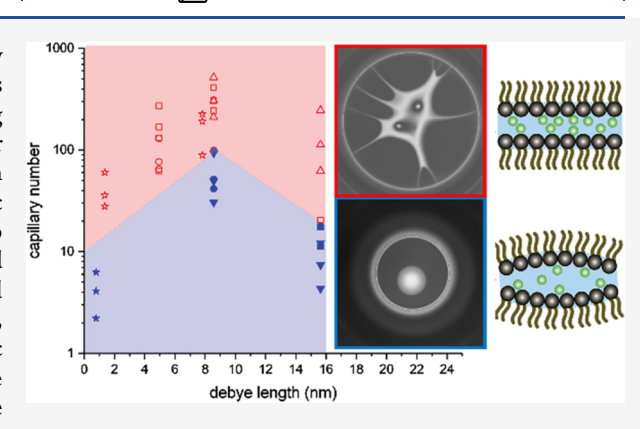
Cite This: Langmuir 2023, 39, 16294-16302



**ACCESS** I

Metrics & More

**ABSTRACT:** While the use of lipid nanoparticles in drug delivery applications has grown over the past few decades, much work remains to be done toward the characterization and rational design of the drug carriers. A key feature of delivery is the interaction of the exterior leaflet of the LNP with the outer leaflet of the cell membrane, which relies in part on the fusogenicity of the lipids and the ionic environment. In this paper, we study the interactions between two lipid monolayers using a thin film balance to create lipid thin films and interferometry to measure film evolution. We probe the role of lipid headgroup chemistry and charge, along with ionic solution conditions, in either promoting or hindering film drainage and stability. Specific headgroups phosphatidylcholine (PC), phosphatidylethanolamine (PE), phosphatidylglycerol (PG), and phosphatidylserine (PS) are chosen to represent a combination of charge and fusogenicity. We



Article Recommendations

quantify each film's drainage characteristics over a range of capillary numbers. Qualitatively, we find that films transition from drainage via a large dimple to drainage via channels and vortices as the capillary number increases. Additionally, we observe a transition from electrostatically dominated film drainage at low CaCl<sub>2</sub> concentrations to fusogenic-dominated film drainage at higher CaCl<sub>2</sub> concentrations for anionic fusogenic (PS) films. Understanding the role of headgroup composition, ionic composition, and ionic concentration will pave the way for the design of tunable vesicle and buffer systems that behave desirably across a range of ex vivo and in vivo environments.

# INTRODUCTION

The cell membrane consists mostly of lipids and proteins, where lipids form a 2D fluid that serves to anchor proteins, direct their function, and maintain the structural integrity of the cell. Lipids are amphiphilic with hydrophobic tails and hydrophilic headgroups, assembling into a bilayer structure with a hydrophobic core. The hydrophobic core is responsible for blocking the passage of ions/large molecules across the bilayer and reducing water permeation while allowing small, uncharged molecules to pass. Thus, proper cell function relies on a variety of ways to transport vital molecules through the barrier.

Cell membrane fusion is one of the methods used to accomplish transport. It involves two separate lipid bilayers merging to form a single continuous membrane, mixing the contents within. This process is orchestrated by a variety of membrane proteins and depends on local membrane composition, temperature, and ionic environment to facilitate intermediate fusion steps. There are 4 major steps typically used to describe fusion: adhesion, hemifusion, formation of fusion pores, and pore enlargement (fusion). The initial stage, adhesion, involves two approaching outer membrane leaflets. As the membranes near each other, the headgroups, proteins,

and ions present begin to influence the interleaflet interactions, ultimately resulting in the mechanical rearrangement and fusion of the bilayers. The fusion process occurs in different contexts: cell—cell fusion, virus-cell fusion, and cell-vesicle fusion. Cell-cell occurs at the earliest stage of propagation for sexually reproducing organisms, with the fusion of sperm-egg membranes, where lipid-anchored proteins also play a role. Virus-cell fusion marks the beginning of viral infection, and the fusion process itself triggers sensing and antiviral response in cells. Cell-vesicle fusion is associated with a variety of physiological and pathological functions such as extracellular vesicles transporting biological cargo molecules, or lipid nanoparticles delivering pharmaceutical agents. All three contexts presented justify the study of membrane fusion although here the study of cell-vesicle fusion is of primary

Received: June 29, 2023
Revised: October 23, 2023
Accepted: October 25, 2023
Published: November 8, 2023





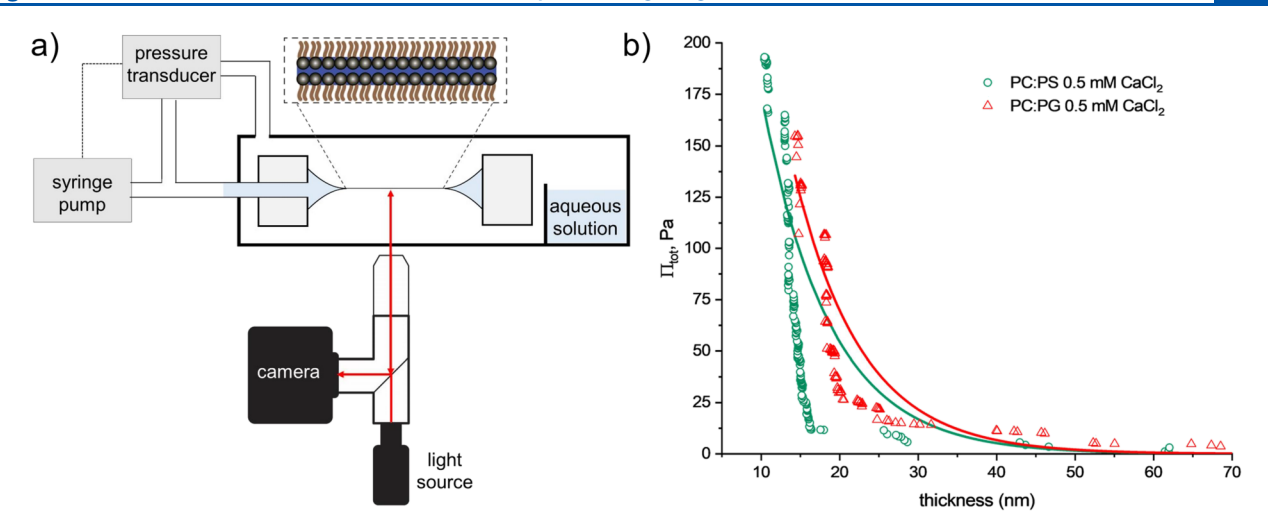


Figure 1. (a) Schematic of the thin film balance experimental setup. (b) Equilibrium disjoining pressure isotherms for 50:50 PC:PS and PC:PG in 0.5 mM CaCl<sub>2</sub>. Lines are fits to the DLVO theory to determine the surface potential, as explained in the text.

interest due to its interesting pathological implications. Drug efficacy can be significantly enhanced through encapsulation within membrane-mimicking vesicles. Advantages include increased systemic circulation, environmentally triggered drug release, and better targeting through biofunctionalization. Whether during the encapsulation process, storage, or in vivo transit, the interactions among a drug carrying vesicle, its cargo, and the target cell membrane must be considered.

Lipid leaflet-leaflet interactions are a factor in the efficacy of drug delivery for liposomal nanoparticles (LNPs). 10 Several competing parameters can affect both the efficacy and stability of LNPs. In the case of drug-carrying liposomes, temperature, membrane tension, fluidity, surface charge, surface modifications (antibodies, PEG), and changes in ionic content alter the vesicle behavior while stored, in transit, and after introduction to the body. Control over membrane composition is critical in maintaining temperature stability in LNP formulations, 11, where storage requirements may limit the accessibility of drug formulations. Modification of the vesicle's surface charge is possible through addition of anionic dioleoylphosphatidylglycerol (DOPG), which has been shown to decrease vesicle stability under electroporation, as opposed to zwitterionic dioleoylphosphatidylcholine. 13 Other headgroups include fusogenic DOPE or DOPS, which promote fusogenic activity in drug carrying liposomes via stabilization of a fusion stalk and interactions with Ca<sup>2+</sup>. 14-16

The vesicle's external ionic environment matters in storage and during drug delivery. The prescence of ions can modify a vesicle's surface properties through association, affecting stability in storage and efficacy during transit. A vesicle is exposed to four major cations during circulation: Na<sup>+</sup> (~145 mM), K<sup>+</sup> (~4.2 mM), Ca<sup>2+</sup> (12.5 mM), and Mg<sup>2+</sup> (~0.8 mM).<sup>17</sup> Of these, Na<sup>+</sup> and Ca<sup>2+</sup> are of particular interest, both due to their relatively high concentration and the latter because of its specific interactions with fusogenic membranes. Asymmetric calcium concentration leads to protein-free membrane fusion in conjunction with fusogenic lipids. <sup>18,19</sup> These ions are present within virtually every target tissue at slightly varying concentrations. Thus, the vesicle's composition and external environment need to be taken into consideration when creating drug carrying LNPs.

To begin to understand how lipid chemistry and ionic solution environment dictates the interactions between lipid

bilayers, we use a modified thin film balance to create, image, and carefully drain an aqueous phospholipid (PL) thin film in air. 20,21 While our previous work loaded oil in the microchip surrounded by an aqueous phase to form a tensionable, <sup>20</sup> freestanding, large area phospholipid bilayer in order to measure membrane Young's modulus and bending rigidity in symmetric, 22 and asymmetric environments, 23,24 here we create inverted phospholipid bilayers in water in order to examine headgroup-headgroup interactions.<sup>25</sup> We suspend the lipids in an aqueous solution and create a thick film (that is subsequently thinned) surrounded by air. In this geometry, the aqueous thin film possesses two opposing lipid monolayers that are brought together during drainage, analogous to the first stage of fusion where opposing lipid leaflets come together. Thin film setups are typically used to study the interactions between capillarity and hydrodynamics in retraction,<sup>26</sup> the effect of ionic strength on film stabilization, <sup>27,28</sup> kinetics of domain expansion, <sup>29,30</sup> and coalescence. <sup>31</sup> In this study, we focus on the effect of increasing NaCl and CaCl<sub>2</sub> concentrations on lipid monolayer interactions. Dioleoyl chains with varied headgroup composition are chosen due to their biological presence, good working temperature range, and existing literature data. The ionic interactions between the films primarily affect the headgroups; however, the acyl chains are left unchanged for consistency. We show how alterations to the thin film composition, by means of different zwitterionic and anionic lipid headgroups, change the film's drainage properties as opposing monolayers approach. The results reported here will ultimately be used to understand what forces drive leaflet stability of a phospholipid thin film during drainage in varied ionic environments.

# MATERIALS AND METHODS

**Materials.** 1,2-Dioleoyl-sn-glycero-3-phosphocholine (DOPC), 1,2-dioleoyl-sn-glycero-3-phosphoglycerol (DOPG), 1,2-dioleoyl-sn-glycero-3-phosphoethanolamine (DOPE), and 1,2-dioleoyl-sn-glycero-3-phospho-L-serine (DOPS) in chloroform were obtained from Avanti Polar Lipids. NaCl and CaCl<sub>2</sub> were purchased from Fisher Scientific. Aqueous buffers were prepared using ultrapure water (Milli-Q, Millipore-Sigma) and filtered through a 200 nm pore filter before use.

**Lipid Mixture Preparation.** Lipids are stored in airtight vials at a 10 mM concentration in chloroform. A small volume of DOPC-chloroform stock is transferred into a 7 mL vial and attached to a gas-

vacuum manifold. First the vial is purged using N2, and then it is dried under vacuum (~30 mbar) overnight, resulting in a thin, dry lipid film. Once dry, the vial is weighed to determine the final mass of lipid. For two-component films, the secondary lipid (DOPG, DOPS, or DOPE) is added to the DOPC-containing vial and dried once again. The dry mixture is reweighed to determine the primary and secondary lipid content. Two-component films are dried together before being resuspended for vesicle consistency. Ultrapure water is added to the dried lipids such that the final concentration is 1 wt % before the solution is sonicated for 4 h to resuspend the lipids. The 1 wt % solution is then used to create three final samples consisting of 0.1 wt % lipid and 1.5, 50, 150 mM NaCl or 0.15, 0.5, and 1.5 mM CaCl<sub>2</sub>. This is done by adding ultrapure water, 1 wt % lipid solution, and concentrated NaCl or CaCl2 stock depending on the desired salt concentration. These aqueous solution conditions were chosen to span a range that is relevant to biological systems while also being adequate to stabilize anionic headgroup films as they drain and transition to common black films, as expanded upon later.

Experimental Setup and Film Thickness Measurement. A bikewheel microfluidic device consisting of a stainless-steel capillary leading into a glass microfluidic chip is used to create a thin film with the desired composition. 21,25 A single channel within the glass chip connects to the capillary tube and then bifurcates. Each resulting channel then leads to opposing sides of a circular chamber containing 24 smaller, radially arranged channels, which lead to an aperture 0.9 mm in diameter. The chip is washed sequentially with ethanol and ultrapure water prior to use. At least 1 mL of the intended sample is cycled through the chip prior to placing the chip into the sample cell. A portion of the sample is added to a separate chamber within the sample cell to mitigate evaporation. The cell is sealed and placed onto a Nikon Ti2 Eclipse to be imaged with monochromatic (640  $\pm$  20 nm) light generated by a Spectra X light engine. A differential pressure transducer (MKS Baratron) controls the disjoining pressure within the microfluidic device using the chamber of the test cell as the reference pressure. A schematic of the experimental setup is shown in Figure 1a.

The thickness of thin films can be determined by imaging the film via monochromatic light or separating white light into RGB components<sup>28</sup> and applying the Sheludko equation:<sup>32</sup>

$$h_{\rm eq} = \left(\frac{\lambda}{2\pi n_{\rm f}}\right) \left[m\pi \pm \arcsin\sqrt{\frac{\Delta}{1 + \frac{4Q(1-\Delta)}{(1-Q)^2}}}\right]$$
(1)

$$Q = \left(\frac{n_{\rm f} - n_{\rm c}}{n_{\rm f} + n_{\rm c}}\right)^2 \tag{2}$$

where  $h_{\rm eq}$  is the equivalent thickness,  $\lambda$  is the wavelength of monochromatic light (640 nm),  $n_{\rm f}$  (1.338) and  $n_{\rm c}$  (1) are the refractive indices of the film (water) and continuous phase (air), respectively, and m is the order of interference.  $\Delta = ({\rm I} - I_{\rm min})/(I_{\rm max} - I_{\rm min})$ , where I is the recorded pixel intensity, and  $I_{\rm min}$  and  $I_{\rm max}$  are minimum and maximum pixel intensities recorded from the interference fringes during the film's drainage. Using this approach, measurements of film thickness can be made with 3 nm resolution. The resolution limit in film thickness is propagated when subsequent parameters are calculated, such as the capillary number explained below.

**Goniometry.** Pendant drop experiments are performed with a Theta optical tensiometer from Biolin Scientific. The surface tension was determined using Attension software. First, freshly sonicated samples are loaded into a clean  $100~\mu\text{L}$  syringe, which is inserted into the tensiometer's syringe holder. The needle tip (0.32 mm OD) is then lowered into a vial containing a small volume of the sample to minimize evaporation. A drop of approximately  $4~\mu\text{L}$  is formed and allowed to stand for 5 min prior to recording. The waiting period allows a PL monolayer to form at the air—water interface, equilibrating the surface tension. Finally, an array of 330 images taken over 30 s is used to calculate the surface tension.

Thin Film Experiments. Two types of film drainage experiments are carried out: dynamic and equilibrium. Dynamic drainage experiments are the result of large stepwise increases in disjoining pressure, which illustrate the kinetics of drainage, while equilibrium experiments consist of very small stepwise increases in disjoining pressure, which allow the film to equilibrate at each step. Each experiment begins by infusing the sample into the microfluidic aperture to create a thick film and finding the zero disjoining pressure condition, where the film is neither infusing nor draining. For equilibrium experiments, the film is drained slowly by increasing the disjoining pressure in steps of 2 Pa every few minutes, maintaining the film at equilibrium. These experiments yield disjoining pressure isotherms for the lipid films, from which the surface potential may be extracted by modeling the electrostatic component of the disjoining pressure,  $\Pi_{\rm el}$ , using DLVO theory.  $^{33}$ 

During dynamic drainage experiments, the disjoining pressure is increased by a nominal value of 50, 100, or 200 Pa from its zero value. The actual magnitude of the pressure step recorded by the pressure transducer is recorded and used in a subsequent analysis. In the case of dynamic experiments, collective film drainage behavior is described by using the capillary number. A film's capillary number represents the complex drainage of a film experiencing capillarity and dimple formation, and is the ratio between the film's viscous forces and the surface tension contribution to film drainage,<sup>34</sup>

$$Ca = \frac{\eta U R_{\text{bw}}^2}{\sigma h^2} \tag{3}$$

Here,  $\eta$  is the viscosity of the film and in the case of 0.1 wt %, relatively low molecular weight lipids in water, a constant value of  $\eta=1$  mPa s is used. U is the characteristic drainage velocity of the film, calculated by measuring the velocity of the lipid thin film areal increase from the beginning of draining to when it reaches its equilibrium area given a specific pressure. Film drainage is a direct result of an increase in disjoining pressure; however, it is secondarily dependent on the lipid and aqueous environments, so U is dependent on both the applied pressure and film properties. The radius of the microfluidic device's central aperture,  $R_{\rm bw}$ , is 0.45 mm. The film surface tension,  $\sigma$ , was determined for each lipid/salt combination through pendant drop experiments, as described above. Finally, h describes the film thickness as determined by eq 1, and it is dictated by the lipid and aqueous environment.

# RESULTS AND DISCUSSION

**Equilibrium Disjoining Pressure Isotherms.** The disjoining pressure isotherm is experimentally determined through measuring the film thickness as the disjoining pressure is increased, allowing equilibration at each step. The disjoining pressure within the film is defined as the sum of the equilibrium intermolecular forces acting between the two lipid monolayers. In DLVO theory, it is comprised of van der Waals' attraction  $(\Pi_{vdW})$  and electrostatic repulsion forces  $(\Pi_{el})$ . Observations of stepwise thinning behavior within film led to the addition of an oscillatory disjoining pressure component  $(\Pi_{os})^{3.5}$  such that the total disjoining pressure is given as

$$\Pi = \Pi_{\text{vdW}} + \Pi_{\text{el}} + \Pi_{\text{os}} \tag{4}$$

Phospholipid films do not undergo stepwise thinning over the set of experimental conditions; therefore, the oscillatory portion of the disjoining pressure can be ignored, leaving  $\Pi_{\rm vdW}$  and  $\Pi_{\rm el}$ . The van der Waals' contribution is a short-range, attractive, component,

$$\Pi_{\text{vdW}} = -\frac{A_{\text{H}}}{6\pi h^3} \tag{5}$$

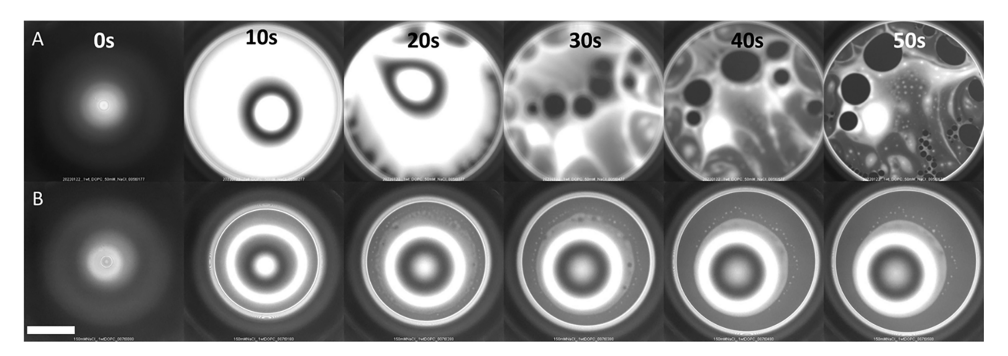


Figure 2. Dynamic thinning of 0.1 wt % DOPC films in solutions of (A) 50 mM ( $\Delta P = 200 \text{ Pa}$ ) and (B) 150 mM NaCl ( $\Delta P = 200 \text{ Pa}$ ). (A) shows drainage through channels and vortices, while (B) shows dimpled drainage. Elapsed time is the same for each series. Scale bar is 200  $\mu$ m.

where  $A_{\rm H}$  is the Hamaker constant and h is the film thickness. The electrostatic contribution depends on the electrolyte's valency, with the following equation, valid for a divalent counterion or divalent co-ion,  $^{33}$ 

$$\Pi_{\text{el}(i:j)} = 432n_2k_BT\tanh^2(\frac{\nu_{i:j}}{4})\exp(-\kappa h)$$
 (6)

where  $n_2$  is the number concentration of divalent ions,  $k_{\rm B}$  is the Boltzmann constant, T is temperature,  $\kappa^{-1}$  is the Debye screening length, and h is the film's thickness. Since the aqueous films are suspended in CaCl<sub>2</sub>, a divalent counterion,

$$v_{i:j}$$
 takes a value of 2:1 as  $v_{2:1} = \ln\left(3/\left(1 + 2\exp\frac{-\varphi e}{k_{\rm B}T}\right)\right)$ , where

 $\phi$  is the film's surface potential and e is the elementary charge. A similar expression exists for monovalent ions. <sup>33</sup>

Films consisting of 1:1 DOPC:DOPS and DOPC:DOPG were drained as described in the previous section, and their disjoining pressure isotherm is shown in Figure 1b. Both films become common black films (h < 20 nm) at low disjoining pressures, but further thinning requires significantly higher pressure due to electrostatic repulsion between monolayers. Fitting eq 6 to the isotherms with the surface potential as the only free fitting parameter yields  $\varphi = -5.4 \pm 0.55$  and  $-4.8 \pm$ 0.63 mV for PC:PG and PC:PS, respectively. PS films are thinner than their PG counterparts, as expected, due to the increased electrostatic repulsion between anionic PG headgroups. However, the quality of the two-term DLVO fit is poor, which we suspect is due to binding of cations to the anionic headgroups or additional structural forces present. Calcium binding constants for POPC:POPG thin films have been reported to be 8.5 M<sup>-1</sup>, whereas those for DOPC:DOPS mixtures have been found to be 650 M<sup>-1</sup>.36,37 This implies greater electrostatic screening for PS films, allowing them to have a decreased disjoining pressure at a given film thickness (said another way, a decreased film thickness at a given disjoining pressure). This specific binding would also contribute to screening the repulsive electrostatic forces between the two monolayers, causing the DLVO prediction to overestimate the disjoining pressure at a given film thickness and underestimate the surface potential. A future consideration may be the addition of a structural disjoining pressure term to the electrostatic and van der Waals attraction terms to improve the model. The addition of other disjoining pressure contribution terms such as hydration  $(\Pi_{hydr})$  and oscillatory  $(\Pi_{os})$  terms has been necessary to describe molecular layering of water between mica plates and stepwise thinning in sodium docecyl sulfate films, respectively.<sup>28,3</sup>

**Dynamic Film Drainage.** Application of a stepwise disjoining pressure increase occurs after bringing the film to an initial  $\Pi = 0$ , where fringes can first be observed. The pressure increase results in rapid film expansion seen in Figure 2, where two DOPC films are being dynamically drained at 50 mM (A) and 150 mM NaCl (B) and  $\Delta P = 211$  and 224 Pa, respectively. This example shows the two main modes of drainage observed in these experiments: channel drainage (A) and dimpled drainage (B). As will be discussed later, the visual drainage characteristics are not only a function of ionic strength but also vary depending on headgroup content, ion valency, and the magnitude of the disjoining pressure step exerted. Channel drainage allows the expansion of common black film domains between "channels" of thicker fluid, where drainage of the liquid occurs. On the other hand, dimpled drainage results in a thick "dimple" appearing at the center of the film, surrounded by a thinner barrier ring.

In the case of channel drainage, the expansion of thinner (darker) domains forcibly drives fluid flow into channels, resulting in faster drainage and a common black film with constant thickness. Alternatively, dimpled drainage resulting from high (150 mM) concentrations of NaCl results in a central portion of the film comprised of a thick, lens-like patch of buffer surrounded by a thinner barrier ring. This phenomenon has been noted in some surfactant systems,<sup>39</sup> and it is attributed to a depletion of surfactant within the film interior due to diffusion. A high ionic concentration enables the formation of a barrier ring due to highly screened electrostatic repulsion at the film's periphery coupled with an abundance of surfactant. The barrier ring imposes hydrodynamic resistance by forcing fluid outflow through a thin radially symmetric channel (A), as opposed to the few thick channels present in (B).

We studied the effect of sodium chloride concentrations from 1.5 to 150 mM (approximately the concentration of NaCl in blood) on film drainage properties of DOPC, using three different magnitude step increases in pressure for each, and find the capillary number from eq 3 (Figure 3). For each ionic strength, the capillary number increased with increasing  $\Delta P$ , primarily due to the increased velocity of film expansion, U. The capillary number of the DOPC film decreased with increased sodium chloride concentration while undergoing a transition in its mode of drainage as shown in Figure 3.

The change in Ca with ionic strength is a result of changing surface tension and the common black film thickness. The surface tensions of DOPC monolayers increase from 59 to 72 mN/m as the ionic strength increases from 0.5 to 150 mM. This increase is likely a result of excess ions disrupting

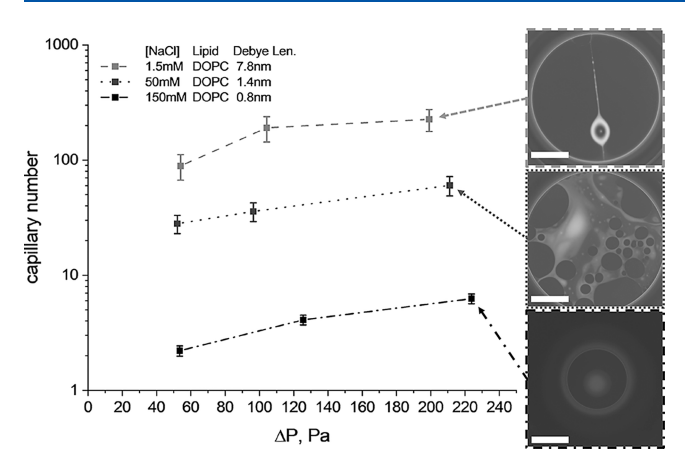


**Figure 3.** Capillary number for dynamically drained DOPC films at different ionic solution conditions and  $\Delta P$ . Images on the right show the different modes of drainage that occur concurrently with modifying drainage capillary number. Scalebar is 200  $\mu$ m.

monolayer formation at the air—water interface. Small concentrations of surfactant (SDS) have been shown to reduce surface mobility in water. In our case, an increased sodium chloride concentration reduces the film's surface mobility. The combination of increased surface tension and surface immobilization leads to a lower overall capillary number as the concentration of NaCl increases. With this base case of a zwitterionic lipid in monovalent NaCl, we proceed to examine the effect of changing headgroup chemistry in divalent (CaCl<sub>2</sub>) solutions.

Films consisting of DOPC and 1:1 PC:PE, PC:PG, PC:PS were drained dynamically at nominal pressure steps of 50, 100, and 200 Pa and calcium chloride concentrations of 0.15, 0.5, and 1.5 mM. These conditions were chosen such that the range of Debye lengths overlap with the aforementioned NaCl films and are in a biologically relevant regime where divalent cations, specifically calcium, are expected to possess specific lipid headgroup interactions that drive adhesion and fusion.<sup>41</sup>

At a concentration of 0.5 mM CaCl<sub>2</sub>, films are divided into two sets of film thicknesses as seen in Figure 4. Anionic films containing PG or PS were thicker than films containing zwitterionic PC or PE. This is analogous to the introduction of anionic DMPG to DOPC films that has been found to increase film thickness attributed to an increase in the repulsive component of the disjoining pressure. 42 This electrostatic repulsion effect presents itself both in the final thickness of the film and in capillary numbers of anionically charged inverted bilayers. Equation 6 can be used to determine the electrostatic portion,  $\Pi_{e\nu}$  of the total disjoining pressure using the surface potential determined from the equilibrium fit in Figure 1 ( $\phi_{PG}$ = -5.4 mV,  $\varphi_{PS}$  = -4.8 mV) at the thicknesses shown in Figure 4 ( $h_{PG} = 21$  nm and  $h_{PS} = 17$  nm). With a CaCl<sub>2</sub> concentration of 0.5 mM, this results in values of  $\Pi_{el\ PG}$  = 68 Pa for the DOPC:DOPG film and  $\Pi_{el\_PS} = 76 \text{ Pa}$  for the DOPC:DOPS film. While the presence of calcium decreases  $\Pi_{\rm el}$  by screening electrostatic repulsion at the film's surface, it still makes up a significant portion of the applied 200 Pa disjoining pressure, leading to an overall higher thickness when compared to zwitterionic films.

Studies of DMPC films in ethanol/water mixtures have concluded that zwitterionic film stability is mostly determined by structural forces. 43,44 However, charging of the air-water interface in zwitterionic lipid films can occur, 45,46 and is attributed to positive specific adsorption of hydroxide ions. A mildly charged surface is likely responsible for the higher thicknesses of the PC and PE bilayers at low calcium concentrations. Decreased thickness at a CaCl<sub>2</sub> concentration of 0.5 mM can be attributed to the presence of cations outcompeting OH<sup>-</sup> surface binding, screening a portion of the electrostatic disjoining pressure contribution. This aligns with pH dependent surface tension data of PE monolayers, which show a decrease in headgroup area and lower surface tension below from pH 9 to pH 4.47 We suspect the effect of increasing CaCl<sub>2</sub> to be similar to that of decreasing pH: the higher concentrations of Ca2+ would cause a decrease in OHadsorption. The subsequent decrease in headgroup area can

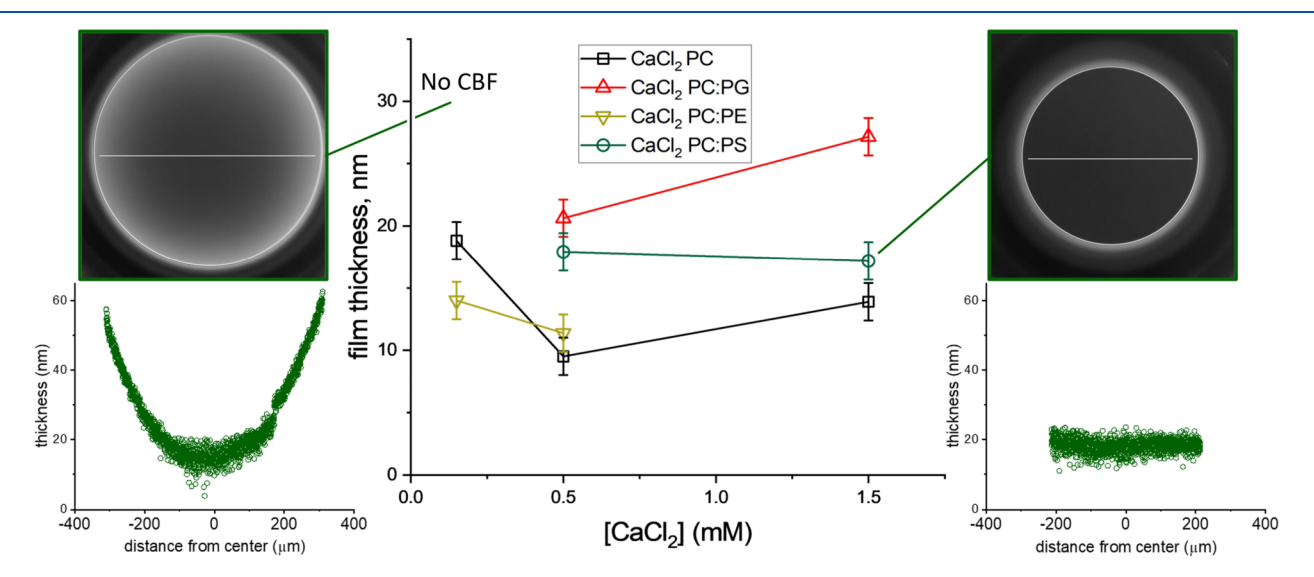
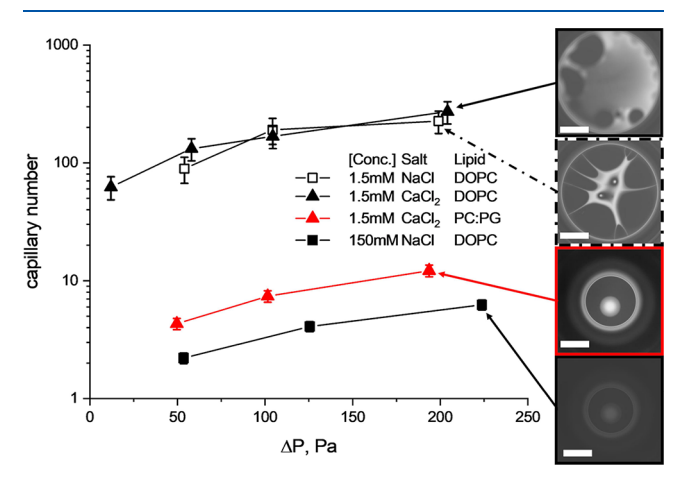


Figure 4. Film thickness as a function of the calcium concentration and headgroup charge. Low calcium concentrations are sufficient to stabilize zwitterionic common black films, but not anionic ones. Line scans of DOPC:DOPS films formed in 0.15 and 1.5 mM  $CaCl_2$  are shown on the left and right, respectively. Low concentrations of divalent cation coupled with a negatively charged surface prevents the common black film transition (left) while increased cation results in common black film formation (right). DOPE films are short-lived in 1.5 mM  $CaCl_2$  due to extensive lipid aggregation.

then induce a negative spontaneous curvature on PE films. Surface binding studies for divalent cations have found concentrations of up to 1 mM Ca<sup>2+</sup> decrease (less negative) the zeta potential of DOPS:DMPS 2 mg/mL vesicle solutions of pH = 7.1 and 10 mM KCl.<sup>48</sup> For comparison, our bulk DOPS concentrations were  $\sim$ 5.2 mg/mL with pH = 7.4 and no other ions. Therefore, we expect the contribution of  $\Pi_{el}$  to anionic (PG, PS) films to be significantly higher at a CaCl<sub>2</sub> concentration of 0.15 mM. In fact, the anionic PG and PScontaining films are unable to transition to common black films at applied pressure steps of up to 200 Pa at this concentration. PC:PS film at this low CaCl<sub>2</sub> concentration had nonuniform thicknesses that ranged from 60 nm at the edges to 20 nm at the center, as opposed to a constant film thickness of  $\sim 17$  nm for PC:PS in 1.5 mM CaCl<sub>2</sub> (Figure 4 left and right, respectively).

Film composition and ionic effects are also manifested in the dynamic drainage characteristics, as described quantitatively by the capillary number and qualitatively by the mode of drainage. Several exemplary sets of experiments are shown in Figure 5.



**Figure 5.** Capillary number for dynamically drained films with different headgroup chemistries, ionic solution conditions, and  $\Delta P$ . Images on the right show the different modes of drainage that occur concurrently with modifying drainage capillary number. Scalebar is 200  $\mu$ m.

As explained above, increasing NaCl concentration decreases the capillary number for DOPC films concurrent with a transition from channel to dimple drainage. At low ionic concentrations, films do not experience significant electrostatic screening due to ionic surface binding. For example, NaCl and CaCl<sub>2</sub> at a concentration of 1.5 mM ( $\kappa_{CaCl_2}^{-1}$  = 4.9 nm,  $\kappa_{NaCl}^{-1}$  = 7.8 nm), have similar capillary numbers and drainage characteristics (channel drainage). At a constant 1.5 mM CaCl<sub>2</sub> concentration, changing from fully zwitterionic DOPC to a 1:1 mixture of DOPC:DOPG yields in an order of magnitude decrease in the capillary number. This is likely because Ca2+ binds onto the PG phospholipid headgroup, as shown in FTIR binding experiments, 49,50 where the divalent cation is shown to form a complex with the headgroups. HNMR studies have found incorporating PG onto a PC enhances the surface binding of Ca<sup>2+</sup> by approximately a factor of 4 while also suggesting the formation of a ternary complex consisting of two lipids bound to one Ca2+ ion.36

The large difference in capillary numbers between PC and PC:PG films at 1.5 mM Ca<sup>2+</sup> can also be explained by a combination of electrostatic repulsion opposing film thinning and higher local [Ca<sup>2+</sup>] at the film's edge due to enhanced surface binding. The combination of electrostatics and surface binding led to a formation of a barrier ring and dimpled drainage similar to that of 150 mM NaCl DOPC films (also shown in Figure 5). The addition of NaCl serves to *decrease* weak electrostatic repulsion in the DOPC case, resulting in a decreased capillary number. In turn, the incorporation of anionic DOPG served to *increase* monolayer electrostatic repulsion, with the capillary number also decreasing as a result.

When dynamically draining pure DOPC films and 1:1 mixtures of PC:PE, PC:PG, and PC:PS, we observed a similar trend in their capillary number as we did in thicknesses at a concentration of 0.5 mM CaCl<sub>2</sub> (Figure 6a). The films separate into anionic and zwitterionic groups with regards to their capillary number, with films containing anionic headgroups having a lower capillary number at a given drainage condition. While this is not so surprising since thickness is used to calculate capillary number, the films also showed a significant difference in their drainage velocity (*U*), depending on charge.

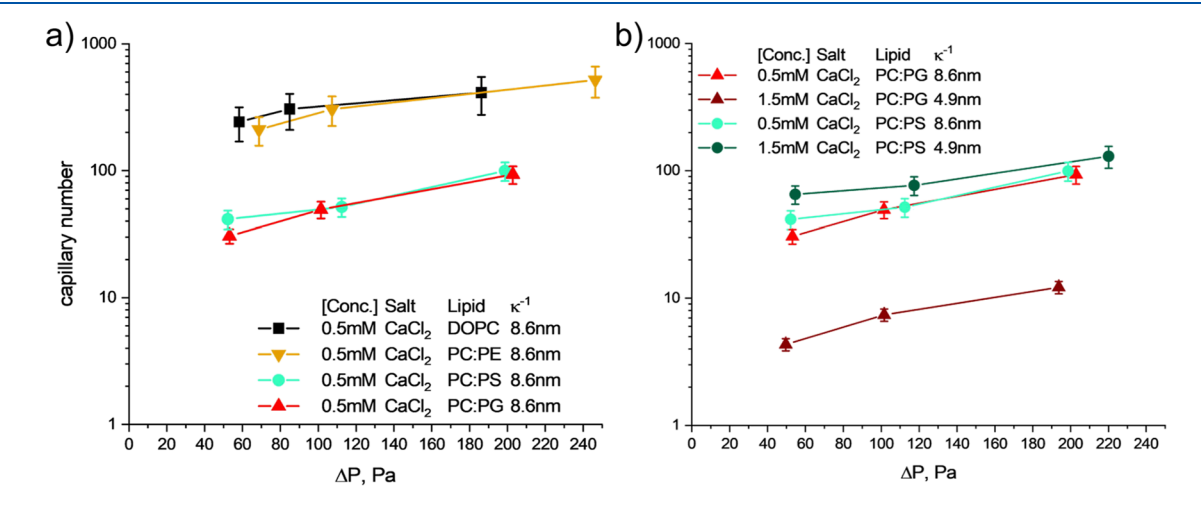
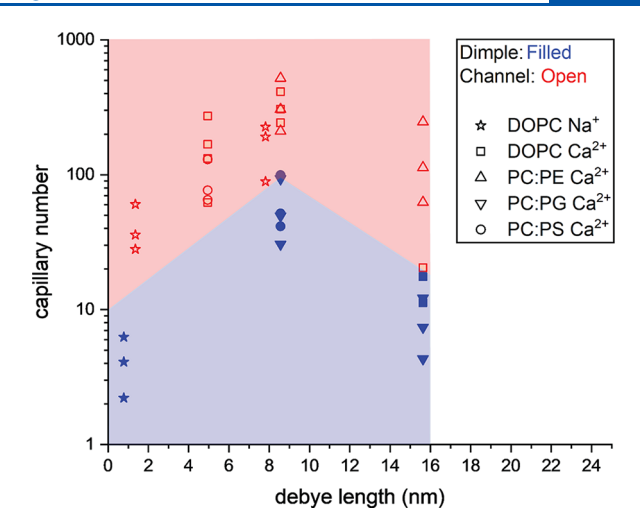


Figure 6. Capillary number for dynamically drained films with different headgroup chemistries at (a) 0.5 mM CaCl<sub>2</sub> and (b) anionic headgroup containing films (PC:PG and PC:PS). Drainage of varied headgroup films (left) is determined by headgroup charge in 0.5 mM CaCl<sub>2</sub>, while films behave differently depending on their fusogenic status at higher CaCl<sub>2</sub> concentrations (right).

Bulk lipid concentrations within the film solution were approximately 13 mM ([lipid]/[Ca<sup>2+</sup>] = 26). This means that Ca<sup>2+</sup> binding is likely proportional to the concentration of calcium near the pure DOPC monolayer, and higher than the initial bulk concentration.<sup>37</sup> Zwitterionic lipids are thought to play a role in increasing local (unbound) Ca<sup>2+</sup>. Thus, even small additions of negatively charged lipid headgroups, such as PS or PG, enhance Ca<sup>2+</sup> surface binding by 2 orders of magnitude, as shown in NMR studies.<sup>51</sup> At a concentration of 0.5 mM, however, cationic binding is unlikely to fully compensate for the negative membrane surface charge.

Interestingly, at Ca<sup>2+</sup> concentrations of 1.5 mM ([lipid]/  $[Ca^{2+}] = 8.7$ ), we observe a divergence between anionic nonfusogenic (PG) and anionic fusogenic films (PS) (Figure 6b). Anionic, nonfusogenic PG-containing films show decreased capillary numbers, resulting from both an increased film thickness and a reduction in the drainage velocity. The reduced drainage velocity can be explained by a reduction in the lateral mobility of DOPG.<sup>52</sup> Anionic, fusogenic PScontaining films increase in capillary number. The increase is due to a higher surface velocity coupled with a marginally lowered thickness. Calcium binds to both headgroups, 36,37 so the divergence in capillary numbers could be due to altered surface potentials, specific orientation of the lipids during film expansion as a result of Ca<sup>2+</sup>-induced conformational changes, the additional interaction site for Ca2+ present in PS but not PG headgroups,  $^{53}$  or additional surface forces besides  $\Pi_{el}$ . A change in the spontaneous monolayer curvature may be one such conformational change as DOPS is initially cylindrical, with a packing parameter of ~1 creating planar monolayers. As more calcium binds to the PS headgroup, the area per lipid decreases,<sup>55</sup> and the lipid geometry becomes conical, with a packing parameter >1. Such negative spontaneous membrane curvature could contribute to accelerated film drainage and promote membrane remodeling processes, such as fusion, within the cell membrane. Studies using SDS and Mg<sup>2+</sup> films have found addition of Mg2+ beyond a critical value to destabilize films by increasing the ionic correlation attraction  $(\Pi_{corr})^{33}$  A similar phenomenon could be the cause for film destabilization in fusogenic films, thus the rapid drainage rates and reduced film stability for PE and PS films at higher  $[Ca^{2+}]$ .

Finally, Figure 7 summarizes the capillary numbers and qualitative drainage characteristics for all films as a function of Debye length. The highest capillary numbers for each film occur at  $\kappa^{-1} = 7.8$  ([NaCl] = 1.5 mM) and 8.6 nm ([CaCl<sub>2</sub>] = 0.5 mM). Lower Debye lengths result in lower capillary numbers and dimpled drainage simultaneously, attributed to reduced surfactant mobility and increased surface tension coupled with higher ionic concentrations, stabilizing the barrier ring around the film by reducing  $\Pi_{el}$  (electrostatic screening). Higher Debye lengths in nonfusogenic films give rise to a broad range of capillary numbers that are mostly determined by electrostatic repulsion, as evidenced by the order of magnitude difference between PC:PE and PC:PG at  $\kappa^{-1}$  = 15.6 nm. The local maximum in capillary number points to an optimal range of ionic concentrations for maximum rates of film drainage, which strikes a balance between long-range electrostatic repulsion and rapid thinning/stabilization of a film's periphery. Low ionic concentrations are required to stabilize the formation and subsequent drainage of the film but are not enough to screen electrostatic repulsion within the monolayers. High ionic concentrations are effective in screening electrostatic repulsion; however, the monolayer



**Figure** 7. Film capillary number and mode of drainage for all films. Symbol color and fill correspond to the visual drainage characteristics of each film, while the symbol shape denotes the lipid and ionic content.

surface is disrupted and surface tension increases due to ion-headgroup binding. The local maximum is present in both fusogenic and nonfusogenic films, although the specific value for the ionic concentration depends on the headgroup composition, ionic valency, and lipid concentration. Despite the specific compositional characteristics of each film, a clear visual pattern emerges: dimpled films drain slowly, and channel films drain the fastest.

### CONCLUSIONS

In this work, we created thin lipid films consisting of PC, PE, PG, and PS headgroups to explore their dynamic drainage based on salt concentration and headgroup charge/fusogenicity. We have shown differences in drainage depending on both the solution and film characteristics. Low drainage rates at high Debye lengths,  $\kappa^{-1}$  are attributed primarily to electrostatic repulsion. Low drainage rates at low  $\kappa^{-1}$  values are attributed to a combination of surfactant mobility, increased surface tension, and stabilization of a barrier ring due to screening. These combined effects give rise to dimpled drainage at low capillary numbers, where the barrier ring traps a large portion of fluid within the center of the film. Finally, the fusogenic status of a lipid (DOPS) increases the drainage rate beyond a [CaCl<sub>2</sub>] threshold somewhere between 0.5 and 1.5 mM. The DOPS film behavior is a reversal in trend when compared to all other films and points to structural forces in addition to electrostatics acting upon phospholipid films. It is possible that the amount of surface-bound Ca2+-PS is enough at these concentrations to transition DOPS from a cylindrical shape, (packing parameter =  $\sim$ 1) to a conical shape (packing parameter >1) which can potentially promote processes that involve membrane deformation. The emergence of structural forces as the main driving factor in DOPS film thinning beyond 0.5 mM CaCl<sub>2</sub> is further reinforced by the Ca<sup>2+</sup> DMPS:DOPS binding and permeation studies. Binding studies suggest little dependence of surface charge, while permeation experiments suggest crystallization of acyl chains beyond 1 mM ĈaCl<sub>2</sub>. 48,56

The interactions between membranes and cations such as calcium and sodium are important in understanding not only biological processes but also the stability of LNP formulations. Capillary numbers obtained from simple drainage experiments

will enable further study of complex lipid film interactions across a range of salt concentrations and lipid compositions. In the future, complex multicomponent lipid films with additional biomolecules can be formed to mimic exosome-cell membrane adhesion and fusion. Understanding headgroup interactions in the context of complex protein-free films can thus inform lipid selection for selective, compositionally dependent fusion. This would in turn facilitate either maximizing or minimizing interactions between vesicles during storage or vesicles and cellular membranes in vivo.

#### AUTHOR INFORMATION

#### **Corresponding Author**

Peter J. Beltramo – Department of Chemical Engineering, University of Massachusetts Amherst, Amherst, Massachusetts 01003, United States; orcid.org/0000-0003-3837-4457; Email: pbeltramo@umass.edu

#### Author

Oscar Zabala-Ferrera — Department of Chemical Engineering, University of Massachusetts Amherst, Amherst, Massachusetts 01003, United States

Complete contact information is available at: https://pubs.acs.org/10.1021/acs.langmuir.3c01795

#### **Author Contributions**

P.J.B. designed and planned the research. O.Z.-F. performed the experiments and analyzed the experimental results. O.Z.-F. and P.J.B. wrote the manuscript and have given approval to the final version of the manuscript.

# **Funding**

Funding for this research was provided in part by the National Science Foundation under award no. CBET-1942581 and by the University of Massachusetts, Amherst.

#### Notes

The authors declare no competing financial interest.

# ACKNOWLEDGMENTS

The authors acknowledge the University of Massachusetts Institute for Applied Life Sciences Advanced Digital Design and Fabrication facility for assistance in fabricating sample cells used in this work.

#### REFERENCES

- (1) Zimmerberg, J.; Chernomordik, L. V. Membrane Fusion. *Adv. Drug Deliv. Rev.* **1999**, 38 (3), 197–205.
- (2) Stein, K. K.; Primakoff, P.; Myles, D. Sperm-Egg Fusion: Events at the Plasma Membrane. J. Cell Sci. 2004, 117 (26), 6269–6274.
- (3) Holm, C. K.; Jensen, S. B.; Jakobsen, M. R.; Cheshenko, N.; Horan, K. A.; Moeller, H. B.; Gonzalez-Dosal, R.; Rasmussen, S. B.; Christensen, M. H.; Yarovinsky, T. O.; Rixon, F. J.; Herold, B. C.; Fitzgerald, K. A.; Paludan, S. R. Virus-Cell Fusion as a Trigger of Innate Immunity Dependent on the Adaptor STING. *Nat. Immunol.* **2012**, *13* (8), 737–743.
- (4) Prada, I.; Meldolesi, J. Binding and Fusion of Extracellular Vesicles to the Plasma Membrane of Their Cell Targets. *Int. J. Mol. Sci.* **2016**, *17* (8), 1296.
- (5) Kumar, S.; El-Hage, N.; Batrakova, E. Extracellular Vesicles in HIV, Drug Abuse, and Drug Delivery. *J. Neuroimmune Pharmacol.* **2020**, 15 (3), 387–389.
- (6) Luk, B. T.; Zhang, L. Cell Membrane-Camouflaged Nanoparticles for Drug Delivery. *J. Control. Release* **2015**, 220, 600–607.

- (7) Wilhelm, S.; Tavares, A. J.; Dai, Q.; Ohta, S.; Audet, J.; Dvorak, H. F.; Chan, W. C. W. Analysis of Nanoparticle Delivery to Tumours. *Nat. Rev. Mater.* **2016**, *1* (5), 16014.
- (8) Hasan, T.; Kawanishi, R.; Akita, H.; Nishikawa, Y. Toxoplasma Gondii GRA15 DNA Vaccine with a Liposomal Nanocarrier Composed of an SS-Cleavable and PH-Activated Lipid-like Material Induces Protective Immunity against Toxoplasmosis in Mice. *Vaccines* **2022**, *10* (1), 21.
- (9) Goswami, R.; O'Hagan, D. T.; Adamo, R.; Baudner, B. C. Conjugation of Mannans to Enhance the Potency of Liposome Nanoparticles for the Delivery of Rna Vaccines. *Pharmaceutics* **2021**, *13* (2), 240.
- (10) Nakamura, T.; Yamada, K.; Sato, Y.; Harashima, H. Lipid Nanoparticles Fuse with Cell Membranes of Immune Cells at Low Temperatures Leading to the Loss of Transfection Activity. *Int. J. Pharm.* 2020, 587, No. 119652.
- (11) Drazenovic, J.; Ahmed, S.; Tuzinkiewicz, N.-M.; Wunder, S. L. Lipid Exchange and Transfer on Nanoparticle Supported Lipid Bilayers: Effect of Defects, Ionic Strength, and Size. *Langmuir* **2015**, 31 (2), 721–731.
- (12) Ban, C.; Lim, S.; Chang, P. S.; Choi, Y. J. Enhancing the Stability of Lipid Nanoparticle Systems by Sonication during the Cooling Step and Controlling the Liquid Oil Content. *J. Agric. Food Chem.* **2014**, 62 (47), 11557–11567.
- (13) Lira, R. B.; Robinson, T.; Dimova, R.; Riske, K. A. Highly Efficient Protein-Free Membrane Fusion: A Giant Vesicle Study. *Biophys. J.* **2019**, *116* (1), 79–91.
- (14) Haque, M. E.; McIntosh, T. J.; Lentz, B. R. Influence of Lipid Composition on Physical Properties and Peg-Mediated Fusion of Curved and Uncurved Model Membrane Vesicles: "Nature's Own" Fusogenic Lipid Bilayer. *Biochemistry* 2001, 40 (14), 4340–4348.
- (15) Sun, S.; Wang, M.; Alberti, K. A.; Choy, A.; Xu, Q. DOPE Facilitates Quaternized Lipidoids (QLDs) for in Vitro DNA Delivery. *Nanomedicine* **2013**, *9*, 849–854.
- (16) Wiseman, D. J.; Cordeiro, C.; Finlay, B. B.; Webb, M. S.; Cordeiro, C.; Finlay, B. B.; Webb, M. S. Monogalactosyldiacylglycerol Confers Fusogenicity to Liposomal Delivery Systems and Facilitates Targeting to Hepatocytes. *J. Liposome Res.* **1999**, *9*, 461–475.
- (17) Covington, A. K.; Robinson, R. A. References Standards for the Electrometric Determination, with Ion-Selective Electrodes, of Potassium and Calcium in Blood Serum. *Anal. Chim. Acta* 1975, 78 (1), 219–223.
- (18) Chanturiya, A.; Scaria, P.; Woodle, M. C. The Role of Membrane Lateral Tension in Calcium-Induced Membrane Fusion. *J. Membr. Biol.* **2000**, *176* (1), 67–75.
- (19) Cohen, F. S.; Zimmerberg, J.; Finkelstein, A. Fusion of Phospholipid Vesicles with Planar Phospholipid Bilayer Membranes: II. Incorporation of a Vesicular Membrane Marker into the Planar Membrane. *J. Gen. Physiol.* **1980**, *75* (3), 251–270.
- (20) Beltramo, P. J.; Van Hooghten, R.; Vermant, J. Millimeter-Area, Free Standing, Phospholipid Bilayers. *Soft Matter* **2016**, *12* (19), 4324–4331.
- (21) Cascão Pereira, L. G.; Johansson, C.; Blanch, H. W.; Radke, C. J. A Bike-Wheel Microcell for Measurement of Thin-Film Forces. *Colloids Surf. A Physicochem. Eng. Asp.* **2001**, 186 (1–2), 103–111.
- (22) Beltramo, P. J.; Scheidegger, L.; Vermant, J. Toward Realistic Large-Area Cell Membrane Mimics: Excluding Oil, Controlling Composition, and Including Ion Channels. *Langmuir* **2018**, 34 (20), 5880–5888.
- (23) Liu, P.; Zabala-Ferrera, O.; Beltramo, P. J. Fabrication and Electromechanical Characterization of Freestanding Asymmetric Membranes. *Biophys. J.* **2021**, *120* (9), 1755–1764.
- (24) Zabala-Ferrera, O.; Liu, P.; Beltramo, P. J. Determining the Bending Rigidity of Free-Standing Planar Phospholipid Bilayers. *Membranes* **2023**, *13* (2), 129.
- (25) Beltramo, P. J.; Vermant, J. Simple Optical Imaging of Nanoscale Features in Free-Standing Films. *ACS Omega* **2016**, *1* (3), 363–370.

- (26) Chatzigiannakis, E.; Veenstra, P.; Ten Bosch, D.; Vermant, J. Mimicking Coalescence Using a Pressure-Controlled Dynamic Thin Film Balance. *Soft Matter* **2020**, *16* (41), 9410–9422.
- (27) Kolarić, B.; Förster, S.; Regine, K. V. Prog. Colloid Polym. Sci.; 2000; 115.
- (28) Yilixiati, S.; Rafiq, R.; Zhang, Y.; Sharma, V. Influence of Salt on Supramolecular Oscillatory Structural Forces and Stratification in Micellar Freestanding Films. *ACS Nano* **2018**, *12* (2), 1050–1061.
- (29) Zhang, Y.; Sharma, V. Domain Expansion Dynamics in Stratifying Foam Films: Experiments. *Soft Matter* **2015**, *11* (22), 4408–4417.
- (30) Kemal, S. I.; Uribe Ortiz, C. A.; Sharma, V. Surface Forces and Stratification in Foam Films Formed with Bile Salts. *Mol. Syst. Des. Eng.* **2021**, *6* (7), 520–533.
- (31) Chatzigiannakis, E.; Chen, Y.; Bachnak, R.; Dutcher, C. S.; Vermant, J. Studying Coalescence at Different Lengthscales: From Films to Droplets. *Rheol. Acta* **2022**, *61* (10), 745–759.
- (32) Sheludko, A. Thin Liquid Films. Adv. Colloid Interface Sci. 1967, 1 (4), 391-464.
- (33) Angarska, J. K.; Tachev, K. D.; Kralchevsky, P. A.; Mehreteab, A.; Broze, G. Effects of Counterions and Co-Ions on the Drainage and Stability of Liquid Films and Foams. *J. Colloid Interface Sci.* **1998**, 200 (1), 31–45.
- (34) Chatzigiannakis, E. Thin Liquid Films: Where Hydrodynamics, Capillarity, Interfacial Stresses, and Intermolecular Forces Meet; ETH Zurich, 2021.
- (35) Bergeron, V.; Radke, C. J. Equilibrium Measurements of Oscillatory Disjoining Pressures in Aqueous Foam Films. *Langmuir* **1992**, *8* (12), 3020–3026.
- (36) Macdonald, P. M.; Seelig, J. Calcium Binding to Mixed Phosphatidylglycerol-Phosphatidylcholine Bilayers As Studied by Deuterium Nuclear Magnetic Resonance. *Biochemistry* **1987**, 26 (19), 6292–6298.
- (37) Sinn, C. G.; Antonietti, M.; Dimova, R. Binding of Calcium to Phosphatidylcholine-Phosphatidylserine Membranes. *Colloids Surf. A. Physicochem. Eng. Asp.* **2006**, 282–283, 410–419.
- (38) Israelachvili, J. N.; Pashley, R. M. Molecular Layering of Water at Surfaces and Origin of Repulsive Hydration Forces. *Nature* **1983**, 306 (5940), 249–250.
- (39) Velev, O. D.; Gurkov, T. D.; Borwankar, R. P. Spontaneous Cyclic Dimpling in Emulsion Films Due to Surfactant Mass Transfer between the Phases. *J. Colloid Interface Sci.* **1993**, *159*, 497–501.
- (40) Liu, B.; Manica, R.; Liu, Q. Coalescence of Bubbles with Mobile Interfaces in Water. *Phys. Rev. Lett.* **2019**, 122 (19), No. 194501.
- (41) Ohki, S.; Arnold, K. A Mechanism for Ion-Induced Lipid Vesicle Fusion. *Colloids Surf., B: Biointerfaces* **2000**, *18* (2), 83–97.
- (42) Toca-Herrera, J. L.; Krasteva, N.; Müller, H. J.; Krastev, R. Interactions in Lipid Stabilised Foam Films. *Adv. Colloid Interface Sci.* **2014**, 207 (1), 93–106.
- (43) Brezesinski, G.; Müller, H. J.; Toca-Herrera, J. L.; Krustev, R. X-Ray Diffraction and Foam Film Investigations of PC Head Group Interaction in Water/Ethanol Mixtures. *Chem. Phys. Lipids* **2001**, *110* (2), 183–194.
- (44) Toca-Herrera, J. L.; Müller, H. J.; Krustev, R.; Pfohl, T.; Möhwald, H. Influence of Ethanol on the Thickness and Free Energy of Film Formation of DMPC Foam Films. *Colloids Surf. A. Physicochem. Eng. Asp.* **1999**, *152* (3), 357–365.
- (45) Karraker, K. A.; Radke, C. J. Disjoining Pressures, Zeta Potentials and Surface Tensions of Aqueous Non-Ionic Surfactant/ Electrolyte Solutions: Theory and Comparison to Experiment. *Adv. Colloid Interface Sci.* **2002**, *96* (1–3), 231–264.
- (46) Toca-Herrera, J. L.; Krustev, R.; Muller, H. J.; Mohwald, H. Phospholipid Foam Films Studied by Contact Angle Measurements and Fluorescence Microscopy. *Colloid Polym. Sci.* **2000**, 278 (8), 771–776.
- (47) Petelska, A. D.; Naumowicz, M.; Figaszewski, Z. A. The Influence of PH on Phosphatidylethanolamine Monolayer at the Air/

- Aqueous Solution Interface. Cell Biochem. Biophys. 2013, 65 (2), 229–235.
- (48) Averbakh, A.; Lobyshev, V. I. Adsorption of Polyvalent Cations to Bilayer Membranes from Negatively Charged Lipid: Estimating the Lipid Accessibility in the Case of Complete Binding. *J. Biochem. Biophys. Methods* **2000**, 45 (1), 23–44.
- (49) Yamanaka, T.; Tano, T.; Kamegaya, O.; Exerowa, D.; Cohen, R. D. Effects of Metal Ions on the Equilibrium Thicknesses of Foam Films Stabilized by Lysophosphatidylcholine As Studied by FT-IR Spectroscopy. *Langmuir* 1994, 10 (6), 1871–1876.
- (50) Potvin-Fournier, K.; Lefèvre, T.; Picard-Lafond, A.; Marcotte, C.; Dufresne, C.; Cantin, L.; Salesse, C.; Auger, M. Discriminating Lipid—from Protein—Calcium Binding To Understand the Interaction between Recoverin and Phosphatidylglycerol Model Membranes. *Biochemistry* **2016**, 55 (24), 3481–3491.
- (51) Seelig, J. Interaction of Phospholipids with Ca2+ Ions. On the Role of the Phospholipid Head Groups. *Cell Biol. Int. Rep.* **1990**, *14* (4), 353–360.
- (52) Filippov, A.; Orädd, G.; Lindblom, G. Effect of NaCl and CaCl2 on the Lateral Diffusion of Zwitterionic and Anionic Lipids in Bilayers. *Chem. Phys. Lipids* **2009**, *159* (2), 81–87.
- (53) Pedersen, U. R.; Leidy, C.; Westh, P.; Peters, G. H. The Effect of Calcium on the Properties of Charged Phospholipid Bilayers. *Biochim. Biophys. Acta Biomembr.* **2006**, *1758* (5), 573–582.
- (54) Harayama, T.; Riezman, H. Understanding the Diversity of Membrane Lipid Composition. *Nat. Rev. Mol. Cell Biol.* **2018**, *19*, 281.
- (55) Melcrová, A.; Pokorna, S.; Pullanchery, S.; Kohagen, M.; Jurkiewicz, P.; Hof, M.; Jungwirth, P.; Cremer, P. S.; Cwiklik, L. The Complex Nature of Calcium Cation Interactions with Phospholipid Bilayers. *Sci. Rep.* **2016**, *6* (1), 38035.
- (56) Papahadjopoulos, D.; Vail, W. J.; Newton, C.; Nir, S.; Jacobson, K.; Poste, G.; Lazo, R. Studies on Membrane Fusion. III. The Role of Calcium-Induced Phase Changes. *Biochim. Biophys. Acta* 1977, 465 (3), 579–598.